Electron paramagnetic resonance study of rare-earth related centres in $K_2YF_5:Tb^{3+}$ thermoluminescence phosphors

D. G. Zverev,[1†] H. Vrielinck,[1‡]* E. Goovaerts[2] and F. Callens[1§]

[1] Department of Solid State Sciences, Ghent University, Krijgslaan 281-S1, B-9000 Gent, Belgium

[2] Experimental Condensed Matter Physics, Department of Physics, University of Antwerp, Universiteitsplein 1, B-2610 Antwerpen, Belgium (Etienne.Goovaerts@ua.ac.be)

[†] Dmitry.Zverev@ugent.be

[‡] Henk.Vrielinck@ugent.be

[§] Freddy.Callens@ugent.be (*corresponding author*)

*Postdoctoral Fellow of the Research Foundation Flanders (FWO-Vlaanderen)

ABSTRACT

Rare-earth related centres have been investigated in $K_2YF_5:Tb^{3+}$ crystals, exhibiting thermoluminescence (TL) below and above room temperature (RT), using electron paramagnetic resonance (EPR) spectroscopy at Q (34 GHz) and W-band (94 GHz). The spectra have been studied prior to irradiation, after exposure in the kGy range to X-rays at 77 K and subsequent pulse annealing up to 570 K. In addition to Gd^{3+}, previously studied in detail, we identified Er^{3+} and Yb^{3+} centres as accidental impurities in as-grown crystals and determined their effective *g* tensors. The EPR spectra of irradiated and annealed crystals provide evidence for the production of at least three distinct Tb-related trapped hole centres, two of which could definitely be identified as Tb^{4+}. Hence, we prove that the Tb^{3+} activator ions also act as hole traps in K_2YF_5. Pulse annealing experiments indicate that the TL above RT results from thermal release of electrons, recombining at these Tb^{4+} ions.

KEYWORDS

Electron paramagnetic resonance; EPR; K_2YF_5; thermoluminescence, TL; Tb

1. Introduction

Recent reports on thermoluminescence (TL) of rare-earth (RE) activated K_2YF_5 crystals show that these materials exhibit a strong response to various types of ionizing radiation and hence emerge as promising new materials for highly sensitive TL and/or optically stimulated luminescence (OSL) based radiation detectors [1-10]. The details of the mechanisms of TL and OSL in these systems are, however, not yet fully understood. Such details involve the identification of radiation defects created upon exposure, which either are directly involved in the TL processes as trapped electron or hole state, or limit the efficiency of the system. In particular it has been suggested that RE activator ions can also be involved in charge carrier trapping [11, 12], which might explain the high sensitivity of these crystals, especially at high activator concentration.

TL and OSL measurements give no direct structural information on the defects involved in these processes. Electron paramagnetic resonance (EPR) spectroscopy, on the other hand, is particularly well-suited for identifying trapped hole and electron centres, as many of them are paramagnetic. Our recent EPR studies of Ce^{3+}, Tb^{3+} and Dy^{3+} activated K_2YF_5 allowed us to determine the crystal's orthorhombic space group as *Pnam* and to identify very stable oxygen related trapping centres [13, 14] and various F_2^- type intrinsic trapped hole centres with very limited stability at room temperature (RT) [13, 15]. The question whether the RE^{3+} can also act as electron or hole trap has until now only briefly been addressed [13]. In the present study we have selected the K_2YF_5:Tb^{3+} system in order to find an answer to this specific question. In a low symmetry crystalline environment Tb^{3+}, which has a $4f^8$ ($^7F_6$) ground state configuration, as a non-Kramer's ion is expected to be EPR-silent, but electron (Tb^{2+}, $4f^9$ ($^6H_{15/2}$) or hole (Tb^{4+}, $4f^7$ ($^8S_{7/2}$)) trapping would most probably lead to the production of RE related EPR spectra. We expect this to be a more sensitive method of detecting charge trapping by activator ions than observing the intensity decrease of an activator in an originally EPR active state (e.g. $Ce^{3+} \rightarrow Ce^{2+}$ or Ce^{4+}). In a previous study we, indeed, reported the appearance of very wide and highly anisotropic EPR spectra upon X-ray irradiation of K_2YF_5:Tb^{3+} [13]. The main topic of the present paper is a detailed study of the angular dependence of this spectrum, leading to the identification of (at least) three Tb related centres (see Section 3.2). Prior to irradiation the spectra contain contributions of Gd^{3+}, identified earlier [16], and Er^{3+} and Yb^{3+} impurities, whose EPR characteristics are presented in Section 3.1.

2. Materials and methods

The K_2YF_5:Tb^{3+} crystals, with nominal dopant concentrations of 0.2%, were hydrothermally synthesized at the Institute of General and Inorganic Chemistry of the Russian Academy of Sciences in Moscow (N. M. Khaidukov) as described earlier [3]. The crystals were cut to approximate 1.4×1.4×2 mm^3 dimensions with a diamond wire saw, the long edge corresponding to the crystallographic a, b or c axis, and mounted on a quartz rod (2 mm

diameter) allowing for sample rotation in the magnetic field. The crystal orientation was initially controlled by X-ray diffraction and definitively determined during the fitting of the experimental data. The misalignments of the rotation planes (*ab, ac, bc*) could be determined with an accuracy of 0.2°. The samples were irradiated at RT or 77 K with white radiation from a Philips tungsten anticathode X-ray tube operated at 60 kV and 40 mA, for 20 minutes, corresponding to doses of the order of 20 kGy. Such high doses are necessary to obtain good signal to noise ratio in the EPR spectra.

Q-band (34 GHz) CW–EPR measurements were performed with an Bruker ElexSYS E500 EPR/ENDOR spectrometer equipped with an Oxford CF935 cryostat and an ENDOR system. Except those of Gd^{3+}, all RE-related EPR spectra had to be recorded at ~10 K in order to obtain good signal to noise ratios. High frequency (87.5 kHz) field modulation at amplitudes of 0.1 – 0.5 mT was applied. In pulse annealing experiments, the intensity of various EPR spectral components, measured at 10 K, was followed after 77 K irradiation and subsequent thermal annealing to specified temperatures. For annealing temperatures below 300 K the sample was kept in the EPR cryostat and during annealing (of at least one hour) the TL was monitored by connecting the EPR sample holder to an Ocean Optics QE65000 spectrometer through a quartz rod and fibre. Pulse annealing to T > 300 K (in air, during 900 s and subsequent quench to RT) was performed *ex situ* in a preheated Carbolite muffle oven. For the W-band (94 GHz) measurements a Bruker ElexSys E680 setup, also equipped with an Oxford He flow cryostat was used (modulation: 100 kHz and 0.5 mT, T = 10 K). Simulations of EPR spectra and their angular dependences were performed using the EasySpin libraries in Matlab [17].

3. Results and discussion

3.1. RE impurities

In our previous EPR studies we discovered that next to the RE dopant, K_2YF_5 crystals also contain unintentional RE impurities. The EPR spectra of the Gd^{3+} impurity and Ce^{3+} dopant, occupying regular Y^{3+} positions, were studied in detail (at RT) in Ref. [16] K_2YF_5 has 4 symmetry related YF_7 polyhedra in the unit cell. From the fact that for any magnetic field orientation only two symmetry related Gd^{3+} and Ce^{3+} spectra were observed with EPR, we deduced that these polyhedra have the crystallographic *ab* plane as a mirror plane (point group C_s (= C_{1h})). For centres with this symmetry the number of symmetry related spectra reduces further to one for magnetic field orientations in the *ac* and *bc* planes, which presents an easy means of orienting to these planes. For paramagnetic defects with symmetry lower than C_s (i.e. C_1), at magnetic field orientations out of the three principal crystallographic planes all four symmetry related EPR spectra should be discernable. The Gd^{3+} impurity EPR spectra are visible in the samples prior to and also after X-ray irradiation, as are those of the RE impurities which are described in the remainder of this section. We

assume that these impurities have the 3+ valence state like the Y^{3+} ion they replace. This assumption is confirmed by the analysis of their EPR spectra.

Fig. 1a shows the EPR spectrum of K_2YF_5:Tb^{3+} for a magnetic field orientation close to the a axis, zoomed in on the 120 – 240 mT range. This spectral component consists of an intense central line flanked by 8 lines which are approximately equidistant and about 20 – 30 times less intense. Such a pattern is characteristic for Er^{3+}, which has one magnetic isotope (^{167}Er, I = 7/2, 23% natural abundance) [17]. Theoretically, an intensity ratio between central and satellite lines of 26.9 is expected. The close resemblance with the simulated spectrum in Fig. 1b, using the tabulated natural abundances of the Er isotopes, confirms the assignment to Er^{3+}.

Fig. 1c shows part of the EPR spectrum with the magnetic field in the ab plane, about 60° rotated away from the a direction. It exhibits an intense central line flanked by two approximately ten times weaker satellites and several even weaker features, two of which are clearly seen as a doublet with a smaller splitting. The ratio between the two doublet splittings is approximately 1/3, close to the ratio between the gyromagnetic factors of the two magnetic isotopes of Yb (^{171}Yb, I = 1/2, 14.28 % natural abundance, g_N = 0.98734 and ^{173}Yb, I = 5/2, 16.13 % natural abundance, g_N = -0.27196)[17].The calculated spectrum in Fig. 1d, taking the tabulated natural abundances and g_N ratios for the Yb isotopes explicitly into account, does not perfectly match the experiment, but still renders the assignment of this spectrum to Yb^{3+} very convincing.

Both for Er^{3+} ($4f^{11}$, $^4I_{15/2}$) and Yb^{3+} ($4f^{13}$, $^2F_{7/2}$) Kramer's doublet ground states are expected in low symmetry environments which can be described with an effective spin S = 1/2 if sufficiently separated from the higher-lying doublets. The spin Hamiltonian for the analysis of the angular dependence of the central line of the characteristic hyperfine pattern for each of these ions reduces to only the electronic Zeeman term:

$$\hat{H}_S = \mu_B \vec{B} \cdot \vec{\vec{g}} \cdot \hat{\vec{S}}, \qquad (1)$$

in which μ_B represents the Bohr magneton. The experimental angular dependence of the Er^{3+} and Yb^{3+} EPR spectra in two (practically) perpendicular planes is shown in Fig. 2, along with simulations using the best-fit g tensors for these ions, displayed in Table 1. These parameters are confirmed by W-band measurements of the angular dependence in a plane close to ab (see further Section 3.2, figure 5). The g tensor for Ce^{3+} ($4f^1$, $^2F_{5/2}$) in the same host crystal is included in Table 1 for comparison. For all these ions, in any magnetic field orientation, only two symmetry related spectra are observed. Hence, they have C_s symmetry, as would be expected when they enter the K_2YF_5 lattice on substitutional Y^{3+} positions without nearby lattice distortions. This symmetry is also reflected in their g tensors, which are characterized by three distinct principal values and one tilting angle in the ab plane, the principal g_z direction being parallel to the crystal's c axis. The tilting angles show large variety, which is at first glance rather surprising, given the very similar crystalline

environment for the three ions. It should, however, be borne in mind that the principal *g* values and directions are actually produced by crystal field interaction within the ground state term of the ion and that similarity in these crystal fields is not necessarily directly reflected in the effective *g* tensors. As the HF structure for Yb^{3+} and Er^{3+} could not be followed throughout the complete angular dependence, no HF tensors could be determined for these centres.

3.2 Tb-related radiation-induced centres

Figure 3 shows the low-field part of the EPR spectrum, recorded at 10 K for a magnetic field orientation close to a, after X-ray irradiation at 77 K and subsequent pulse annealing (see Section 2) steps. The annealing temperatures were chosen in accordance with our previous study of F_2^- type trapped hole centres in K_2YF_5 [15]. In that study we found that at 100 K, several V_K-type F_2^- centres are converted into the most stable centre of this type V1, while no TL occurs. At 120 K V1 and V2, an H-type F_2^- centre, undergo a partial decay induced by recombination with thermally released electrons. This process is accompanied by TL. The complete decay of V2 and a partial, induced decay of V1 are observed at 140 K, along with TL. Finally, at 160 K the TL-free complete thermal decay of V1 occurs.

After X-ray irradiation at 77 K and rapid transfer into the cavity (bottom spectrum) highly anisotropic EPR transitions in a wide magnetic field range are observed, which, according to their annealing behaviour and angular dependence (see further) all belong to the same centre, which we label T1. In the subsequent pulse annealing steps its intensity steadily decreases, except in the annealing at 160 K, when holes are thermally released from the V1 centre and the T1 intensity markedly increases. Meanwhile, from 120 K and 140 K onwards, other spectral components, labelled T2 and T3, which are not produced by X-ray irradiation at 77 K, grow in. Also these undergo a very pronounced intensity increase at 160 K. We have checked that these centres are not produced in nominally undoped and Ce^{3+} and Dy^{3+} doped crystals. These observations indicate that the T1 – T3 centres are Tb related and produced through hole capture. For the further annealing above RT (not shown in Fig. 3) problems with reproducible positioning (orienting) of the sample in the cavity render the evaluation of the line intensities more difficult. Nonetheless we could establish an important decrease of the T2 signal intensity for anneal temperatures in the 330 - 430 K range and eventually a complete disappearance around 550 – 575 K.

Figure 4 shows the Q-band angular dependence in three perpendicular planes for T1, whose spectrum could be studied separately from the others, if the crystals were not annealed after irradiation to 77 K. The complex angular dependence in a wide magnetic field range, in which widths and intensities of transitions also vary strongly with orientation, suggests that this centre has high spin and a large zero field splitting (ZFS). This angular dependence could only be analyzed assuming that S = 7/2. Simulations using the isotropic *g* value and ZFS parameters in the spin Hamiltonian:

$$\hat{H}_S = \mu_B \vec{B} \cdot \ddot{g} \cdot \hat{\vec{S}} + \sum_{k=2,4,6} \sum_{q=-k}^{k} B_k^q \hat{O}_k^q \left(\hat{\vec{S}} \right) \quad (2)$$

as given in Table 2, are shown in Fig. 4 as full lines. They agree very well with experiment. In equation (2), the O_k^q represent the extended Stevens operators, expressed in the crystal reference frame taking the *z* direction along the twofold screw axis c, and *x* and *y* along a and b, respectively. For any magnetic field orientation only two symmetry related spectra were observed for this centre, indicating that it has C_s symmetry. This is also reflected in its spin Hamiltonian, for which all B_k^q parameters with odd q vanish. Due to the low thermal stability of this centre, no W-band data are available for it. Recording the temperature dependence of the intensity of the EPR transitions did not allow us to determine the absolute sign of its ZFS parameters. The signs reported in Table 2, for one of the two symmetry related sites, are relative to that of B_2^0. The parameters for the other site are found by changing the sign of B_2^{-2}, B_4^{-2} and B_4^{-4} simultaneously. Based on aforementioned observations and its spin S = 7/2 (see Section 1), we identify T1 as a Tb^{4+} centre ($4f^7$ configuration).

The angular dependence of T2 and T3, which appear simultaneously in samples annealed to RT after X-ray irradiation at 77 K, was recorded in three (approximately) perpendicular planes at Q-band frequencies and one additional plane (close to ab) in W-band. In Fig. 5 the 10 K W-band spectrum for a magnetic field orientation along a is shown. The signals of the RE^{3+} impurities (RE=Er,Yb,Gd) in this spectrum can easily be identified by calculating their resonance field positions using the spin Hamiltonian parameters obtained from the Q-band analysis (Tables 1 and, for Gd^{3+} Table 2, third column). The six most intense narrow lines remaining in the spectrum, exhibiting a doublet splitting (~ 7 mT), are due to the $\Delta M_S = 1$ transitions of T2, for which the high-field limit is approached in W-band. At lower fields several "forbidden transitions" are observed for this centre. The unassigned lines are attributed to T3, for which, in spite of having data at two frequency bands, the analysis using spin Hamiltonians of the type of Equation (2) with S up to 7/2 failed.

In Fig. 6 we show the EPR angular dependence for the T2 component, for which a consistent fitting of the data in the two microwave bands was obtained and S was found again to be 7/2. The *g* and ZFS parameters for this centre are also presented in Table 2. The comparison of signal intensities for various transitions in the spectra recorded in the two microwave frequency bands allowed us to determine the absolute sign of the ZFS parameters in this case. For arbitrary magnetic field orientations, four distinct symmetry related spectra are observed, demonstrating that the centre has C_1 symmetry, and all B_k^q parameters differ from zero. In Table 2 the parameters are again given for one of the symmetry related sites. Those for the other three sites are found by reversing the signs for all B_k^{-2p} (site 2), all $B_k^{+(2p+1)}$ (site 3), or $B_k^{-(2p+1)}$ (site 4) parameters simultaneously.

T2 is also identified as a Tb^{4+} centre. Because T3 is produced in similar circumstances, we believe it to be also Tb^{4+} related. However, as we could not fit it with a spin Hamiltonian as in Equation (2), the T3 component is either not due to a single paramagnetic centre, or it corresponds to coupled paramagnetic ions.

Extra confirmation of our identification of T1 and T2 as Tb^{4+} centres comes from a limited number of literature reports on Tb^{4+} in oxide crystals [18-24]. In these papers, the second-order ZFS parameters for Tb^{4+} centres were found to be typically an order of magnitude larger than those for Gd^{3+} centres in the same (or very similar) environments. Comparing the results in Table 2 with those in Ref. [16] we roughly also find an order of magnitude difference. Contrary to expectations for an S state ion, but in agreement with reports on Tb^{4+} in ThO_2 [19] and CeO_2 [20], we observe that the EPR spectra of T1 – T3 are not detectable at RT. In most of the previous observations of Tb^{4+}, the four-lines hyperfine splitting (^{159}Tb isotope with I = 3/2, 100 % natural abundance) of the EPR transitions served as ultimate proof for the identification. Resolved hyperfine interaction constants ranging from ~11 MHz in $CaWO_4$ [18] to ~100 MHz in $ZrSiO_4$ [22, 23] have been reported in these oxide crystals. For the T1 – T3 centres, no such four-lines splitting is observed. The hyperfine interaction could, however, be buried in the EPR line width of the order of 3 mT, which is due to unresolved interactions with the many magnetic nuclei in K_2YF_5:Tb. Most of the EPR transitions do exhibit a doublet line splitting of about 7 mT (~200 MHz), as can e.g. be seen in Fig. 3. We checked through simulations that this splitting is most likely not due to ^{159}Tb interaction, because a four-lines splitting is always produced, even when quadrupole interaction is taken into account. Electron nuclear double resonance (ENDOR) measurements did not help us in identifying this doublet splitting. It could, e.g., be produced by a strong interaction with a single ^{19}F nucleus.

In view of its C_s symmetry, a hole trapped by a Tb^{3+} dopant ion at an undistorted Y^{3+} position seems a good model for T1. Except for a factor of about 10 in the magnitude of the second-order ZFS parameters, this centre should then very closely resemble the Gd^{3+} centre in K_2YF_5. For the latter centre, a rotation of the crystal frame of 3° around the c axis renders all B_2^q parameters, except for B_2^0 and B_2^2 zero, or in an alternative interpretation of the second-order ZFS Hamiltonian, diagonalises the D tensor ($\hat{\vec{S}} \cdot \vec{\vec{D}} \cdot \hat{\vec{S}} = \sum_{q=-2}^{2} B_2^q \hat{O}_2^q\left(\hat{\vec{S}}\right)$). In the latter reference frame, the direction corresponding to the largest principal D value coincides with the Y–F5 bond direction in the YF_7 polyhedron [16], strongly indicating that the Gd^{3+} for Y^{3+} substitution hardly distorts the lattice. A similar analysis for T1 demonstrates that the direction corresponding to the largest principal D value also lies in the ab plane, but now 63° rotated away from the b axis. This dissimilarity with Gd^{3+} may point to a distortion of the centre in the ab plane and might e.g. be an indication for an in-plane off-centre displacement of the Tb^{4+} ion (about 80 pm ionic radius [25]), which is small in comparison with Y^{3+} (90 pm ionic radius [25]). Tb^{4+} at an Y^{3+} represents an effective positive charge $+e$ in

the lattice. A possible way of explaining the production of the lower symmetry T2 centre at elevated temperatures is via thermally activated association with a lattice defect. Two examples of such defects, which would also produce the right symmetry, are an interstitial F^- ion outside the *ab* mirror plane and a K^+ vacancy. Because the production of the T2 centre starts off at low temperature (~120 K) but does not abruptly take place at a specific temperature, we expect this defect to be quite mobile in the lattice, but to have low abundance with only a moderate long-range attractive force to the Tb^{4+} centre. The exact nature of this defect remains, however, unknown.

Hole trapping by the activator ion and subsequent recombination at this site of thermally released electrons presents an attractive mechanism for TL in these crystals, which is expected to be very efficient because the spatial correlation between trapping and activator centres is automatically fulfilled. As hole trapping by Tb^{3+} already occurs by irradiation at 77 K one may wonder whether only recombination with holes trapped at Tb^{3+} can lead to TL in K_2YF_5:Tb. Our thermal pulse annealing experiments are not conclusive in this respect: because the T1-T3 centres could only be detected far below the annealing temperatures and because at many annealing temperatures several production and annihilation processes of these centres occur simultaneously, the correlation of their EPR intensity with TL is far less straightforward to establish than for the F_2^- centres [15]. The comparison of the decay of the T1 intensity after annealing to 120 and 140 K with the time-integrated TL intensity during these anneals suggest a considerably worse correlation of the TL with T1 than with V1. Hence, a mechanism in which thermally released electrons recombine at intrinsic trapped hole centres after which the recombination energy is transferred to a nearby activator centre, as proposed in Ref. [12], cannot be excluded by the present experiments. The number of EPR intensity data points is, however, too limited to draw firm conclusions on this issue. For the TL occurring above 160 K the T1-T3 centres are the most abundant trapped hole centres observable with EPR in these crystals. Mechanisms in which they are directly involved seem very plausible, especially for the TL above RT where a steady decrease of the T2 signal intensity has been observed.

In this context, a comparison with the TL results by Kui et al. [3] for $K_2Y_{0.99}Tb_{0.01}F_5$ crystals after β irradiation may be instructive. They analyzed the observed TL glow curve in terms of four peaks for which the kinetic parameters (activation energy E_a and frequency factor s) were determined. If we assume in a simple model (first order kinetics, see also [13]) that the Tb^{4+} related centres are the only trapped hole states available and that thermal release of electrons (from four distinct centres) with them produces TL, we may write

$$I_{EPR} = \sum_{i=1}^{4} A_i \exp\left(-t/\tau_i\right) \tag{3}$$

with

$$\tau_i = s_i^{-1} \exp\left(\frac{E_{a,i}}{k_B T}\right) \quad (4)$$

and k_B the Boltzmann constant. We then calculated, using the parameters of [3], the temperatures at which annealing during 900 s would cause a certain component of the intensity to drop by 50%. These correspond to the temperatures at which the half-life of the trapped electron state is 900 s. The results, shown in Table 3, exhibit good qualitative agreement with the thermal bleaching observed for T2 above RT (see Section 3.2). In particular, the final decay of the signal in the 550 – 575 K range agrees remarkably well with predictions for the glow peak 4 in Table 3. To establish the correlation between the concentration of Tb^{4+} centres and the occurrence of TL more convincingly, one would have to monitor a property *in situ* observable during the thermal annealing. In this respect, the Tb^{3+}/Tb^{4+} related optical absorption spectrum of the crystals might be a good candidate. A systematic study of the influence of the radiation dose on the EPR spectra and TL glow curves may provide further valuable information on the role of the T1 – T3 centres in the TL processes below and above RT.

4. Conclusions

From the hyperfine structure and the analysis of the angular dependence of the EPR spectra, recorded at 10 K in as-grown K_2YF_5:Tb^{3+} crystals, we identified Er^{3+} and Yb^{3+} as non-intentional paramagnetic impurities, in addition to the previously studied Gd^{3+}. Both ions were shown to have an effective spin S = 1/2 and C_s site symmetry, indicating that they occupy a regular Y^{3+} position in the lattice.

In the 10 K EPR spectra of crystals irradiated with X-rays at 77 K and subsequently annealed to various temperatures below and above RT, at least three Tb-related centres have been observed. Their intensity increases strongly when holes are thermally released from the intrinsic V1 (F_2^- type) centre, indicating that they are trapped hole centres. Two of them, labelled T1 and T2, were shown to have S = 7/2 and are identified as Tb^{4+} ($^8S_{7/2}$) ions substituting for Y^{3+} and are very probably only different with respect to their charge compensation. The signals labelled as T3 cannot be analyzed with a spin Hamiltonian with S up to 7/2 and hence have a more complex structure or are composite. Our EPR results thus prove that the Tb^{3+} activator ions also act as hole traps in K_2YF_5.

The T2 and T3 centres are not produced upon X-irradiation at 77 K but their intensity gradually grows in the spectra when subsequently annealing the crystals up to RT, while the intensity of T1 decreases, eventually to zero. The thermal decay of T2 and T3 has also been followed in isochronal pulse annealing (900 s) experiments above RT up to 575 K. As the EPR spectral intensities and TL could not be monitored simultaneously during the pulse annealing, the role of the T1 – T3 centres in the TL processes could not be unambiguously determined. However, comparison of our pulse annealing experiments with the results of

previous TL studies suggests that recombination of thermally released electrons at the T2 centre (and probably also T3) emerges as a very plausible mechanism for the TL processes above RT.

Acknowledgements

The authors acknowledge the Research Foundation-Flanders (FWO-Vlaanderen, grant no. G.0116.06) and the Hercules Foundation of Flanders, Belgium (contract AUHA013) for financial support. Professor N. M. Khaidukov (Institute of General and Inorganic Chemistry, Russian Academy of Sciences, Moscow) is gratefully acknowledged for the crystal growth and we thank professor D. Poelman (Lumilab, Department of Solid State Sciences, Ghent University) for the use of the Ocean Optics QE65000 spectrometer.

References

1. J. Marcazzo, M. Santiago, E. Caselli, N. Nariyama, N.M. Khaidukov, Opt. Mater. (Amsterdam, Neth.) 26 (2004) 65-70.
2. L.O. Faria, D. Lo, H.W. Kui, N.M. Khaidukov, M.S. Nogueira, Radiat. Prot. Dosim. 112 (2004) 435-438.
3. H.W. Kui, D. Lo, Y.C. Tsang, N.M. Khaidukov, V.N. Makhov, J. Lumin. 117 (2006) 29-38.
4. J.A. Nieto, N.M. Khaidukov, C.B. Guerrero, J.C.A. Vega, T.R. Montalvo, A.G. Cuellar, J.A.I.D. Gongora, P.R.G. Martinez, Radiat. Eff. Defects Solids 161 (2006) 443-449.
5. M.S. Rasheedy, M.A. El-Sherif, M.A. Hefni, Radiat. Eff. Defects Solids 161 (2006) 579-590.
6. E.C. Silva, N.M. Khaidukov, M.S. Nogueira, L.O. Faria, Radiat. Meas. 42 (2007) 311-315.
7. M.S. Rasheedy, M.A. El-Sherif, M.A. Hefni, Nucl. Instrum. Meth. B 258 (2007) 440-444.
8. J. Azorin-Nieto, N.M. Khaidukov, A. Sanchez-Rodriguez, J.C. Azorin-Vega, Nucl. Instrum. Meth. B 263 (2007) 36-40.
9. J. Azorin, A. Gallegos, T. Rivera, J.C. Azorin, N. Khaidukov, Nucl. Instrum. Meth. A 580 (2007) 177-179.
10. J. Marcazzo, N.M. Khaidukov, E. Caselli, C. Dangelo, M. Santiago, Phys. Status Solidi A 206 (2009) 2593-2598.
11. A.J. Wojtowicz, P. Szupryczynski, W. Drozdowski, J. Alloys Compd. 300 (2000) 199-206.
12. N.Y. Kirikova, A.N. Belsky, B. Chassigneaux, J.C. Krupa, V.N. Makhov, M. Queffelec, Proceedings of Fifth International Conference on Inorganic Scintillators and their Applications (1999), Moscow, Russia, 440.
13. H. Vrielinck, D. Zverev, P.F. Smet, D. Poelman, T. Gregorkiewicz, F. Callens, Mat. Sci. Eng., B 146 (2008) 16-21.
14. D. Zverev, H. Vrielinck, F. Callens, P. Matthys, S. Van Doorslaer, N.M. Khaidukov, Phys. Chem. Chem. Phys. 10 (2008) 1789-1798.
15. D.G. Zverev, H. Vrielinck, P.F. Smet, D. Poelman, F. Callens, Phys. Rev. B 79 (2009) 224110.
16. F. Loncke, D. Zverev, H. Vrielinck, N.M. Khaidukov, P. Matthys, F. Callens, Phys. Rev. B 75 (2007) 144427.
17. EPR/ENDOR Frequency Table, in: Bruker Biospin Almanac, Bruker Analytik GmbH, Rheistetten, 2010, pp. 47-50.
18. R.Y. Abdulsabirov, I.N. Kurkin, Izv. Vyssh. Uchebn. Zaved., Fiz. (1978) 143-145.
19. J.M. Baker, J.R. Chadwick, G. Garton, J.P. Hurrell, Proc. R. Soc. A 286 (1965) 352.

20. Y.S. Greznev, M.M. Zaripov, V.G. Stepanov, Sov. Phys. Solid State 7 (1966) 2937.
21. S. Hansen, B.D. Mosel, W. MullerWarmuth, P.E. Fielding, Z. Naturforsch. A 51 (1996) 885-894.
22. D.R. Hutton, R.J. Milne, J. Phys. C: Solid State Phys. 2 (1969) 2297-2300.
23. M.A. Laruhin, H.J. van Es, G.R. Bulka, A.A. Turkin, D.I. Vainshtein, H.W. den Hartog, J. Phys. Condens. Matter 14 (2002) 3813-3831.
24. W.C. Tennant, R.F.C. Claridge, C.J. Walsby, N.S. Lees, Phys. Chem. Miner. 31 (2004) 203-223.
25. R.D. Shannon, Acta Crystallogr. A 32 (1976) 751-767.

Tables

Table 1: Principal values and tilting angle Θ in the *ab* plane for the *g* tensors of RE^{3+} centres with S = 1/2 in K_2YF_5. The principal g_z direction is oriented along the c axis of the crystal. Θ corresponds to the angle between the principal g_x and a axes. The principal *g* values are ordered in such a way that $g_x < g_y$. The error in the last digit is given as a subscript.

	g_x	g_y	g_z	Θ (°)	Ref.
Ce^{3+}	0.25_5	2.74_2	0.75_2	29.7_5	[16]
Er^{3+}	0.81_5	13.6_3	3.19_2	87.6_3	This work
Yb^{3+}	1.21_2	3.04_2	5.26_4	49.2_3	This work

Table 2: Spin Hamiltonian parameters (ZFS parameters B_k^q in MHz, spectroscopic splitting factor g dimensionless) for the T1 and T2 centres produced by X-ray irradiation in $K_2YF_5:Tb^{3+}$. The *xyz* reference frame for representing the B_k^q parameters/$\hat{\mathrm{O}}_k^q$ extended Stevens operators is chosen such that *z* is collinear with the twofold screw axis of the crystal c, *x* is along a and *y* along b. The parameters for Gd^{3+} at 10 K (slightly different from those at RT given in Ref. [16]) are presented for comparison.

	T1	T2	Gd^{3+}
B_2^0	-1523_{20}	-4787_{25}	-548_4
$B_2^{\pm1}$	0	534_{203} -8233_{137}	0
$B_2^{\pm2}$	7197_{75} 10109_{56}	2019_{18} 612_{30}	-1121_7 -80_{11}
B_4^0	4.5_4	$-0.6_{0.3}$	$-0.6_{0.1}$
$B_4^{\pm1}$	0	$-9.7_{5.4}$ $1.8_{2.4}$	0
$B_4^{\pm2}$	$26.3_{2.4}$ $-11.7_{1.9}$	$8.3_{1.4}$ $11.6_{2.2}$	$-2.3_{0.3}$ $-5.4_{0.7}$
$B_4^{\pm3}$	0	$-28.5_{14.0}$ $15.3_{6.4}$	0
$B_4^{\pm4}$	$-30.3_{4.8}$ $-32.3_{3.9}$	$1.3_{1.7}$ $-2.7_{2.9}$	$-3.5_{0.4}$ $1.4_{0.6}$
g	2.002_6	1.993_9	1.990_1

Table 3: Kinetic parameters and temperatures ($T_{1/2}$) corresponding to a half-life of 900 s for the centres whose decay initiates TL for the various glow peaks observed in $K_2YF_5:Tb^{3+}$ (1%) after β-irradiation [3].

Peak no.	**E_a (eV)**	**s (10^9 Hz)**	**$T_{1/2}$ (K)**
1	0.66	0.73	314
2	0.89	4.8	351
3	1.06	2.5	427
4	1.41	7.0	549

Figures

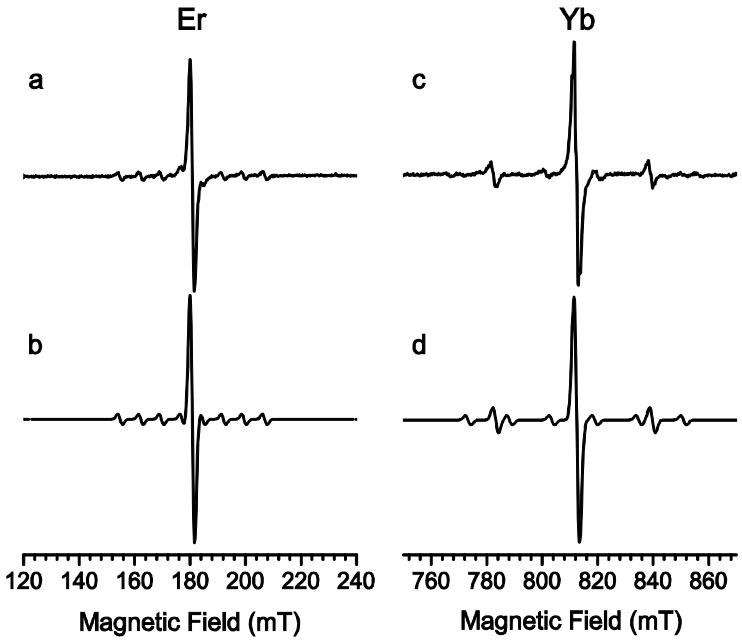

Figure 1 : EPR spectra of RE^{3+} impurities with effective spin S = 1/2 in K_2YF_5, recorded at 10 K, normalized to 34.00 GHz and simulated using natural abundances and tabulated ratios [17] between hyperfine constants for the various isotopes.

a) Experimental, B ∥ a axis, 120 – 240 mT range
b) Simulation, g_{eff} = 13.43, A(^{167}Er) = 1400 MHz
c) Experimental, B in the ab plane, 60° from the a axis, 750 – 870 mT range
d) Simulation, g = 2.99, A(^{171}Yb) = 2363 MHz

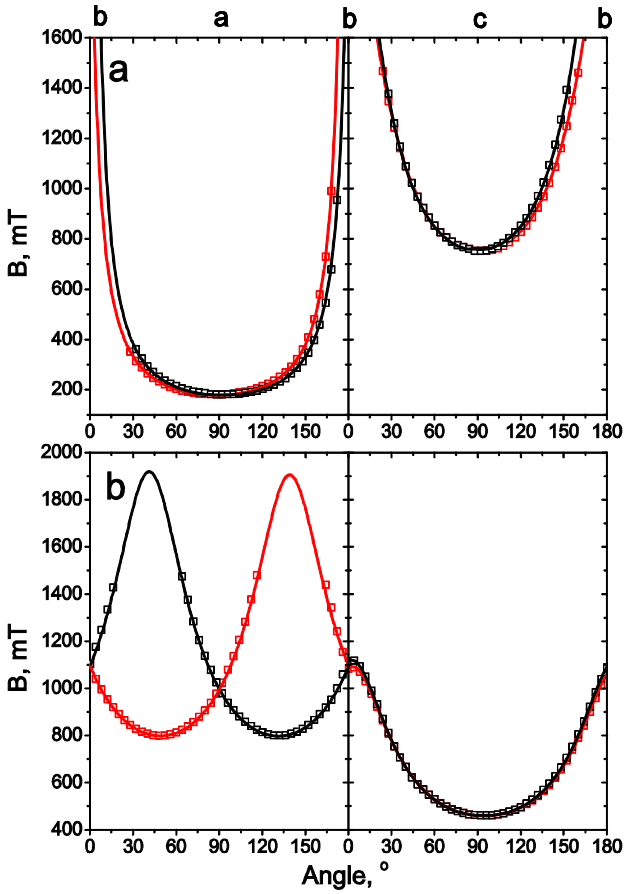

Figure 2 : Angular dependence of the central EPR line positions (symbols), recorded in two nearly perpendicular planes, close to ab and bc, for Er^{3+} (a) and Yb^{3+} (b). Full lines represent simulations using the *g* tensors in Table 1. The principal g_x and g_y directions are tilted away from the crystal axes in the ab plane (see Table 1), as a result of which two symmetry related sites (different colours/symbols) can be distinguished in the bab rotation plane (left panels). In the bcb plane the spectra of the two sites should in principle coincide, but due to a small misalignment of the rotation plane, for certain orientations the site splitting is still resolved.

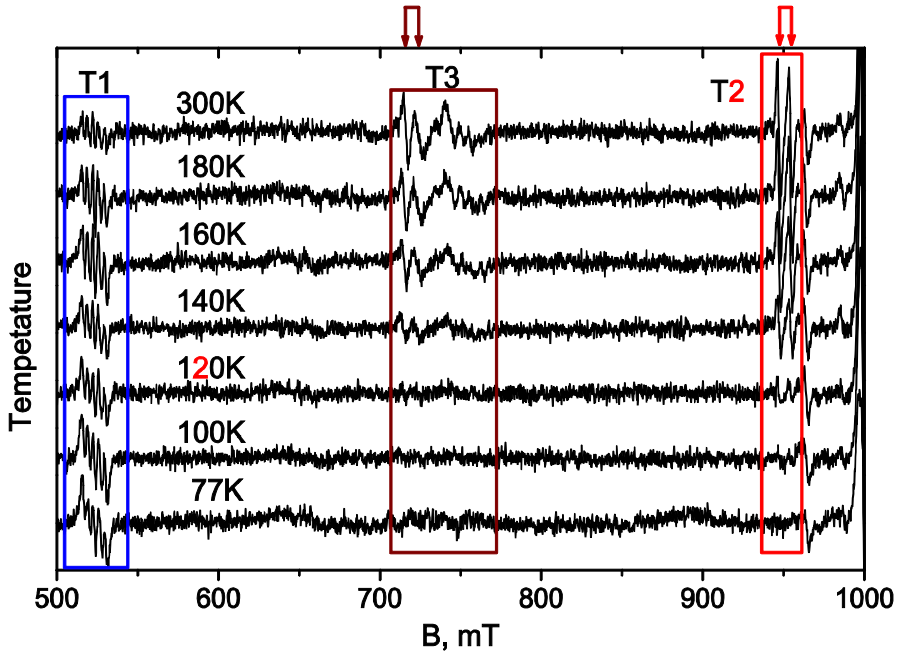

Figure 3: Transformation of the Q-band EPR spectrum of K_2YF_5:Tb^{3+} after X-ray irradiation at 77 K, recorded at 10K (magnetic field orientation along the a-axis) as a function of the annealing temperature (indicated). The doublet splitting of ~7mT (200 MHz, see text) in the T2 and T3 components is indicated with arrows.

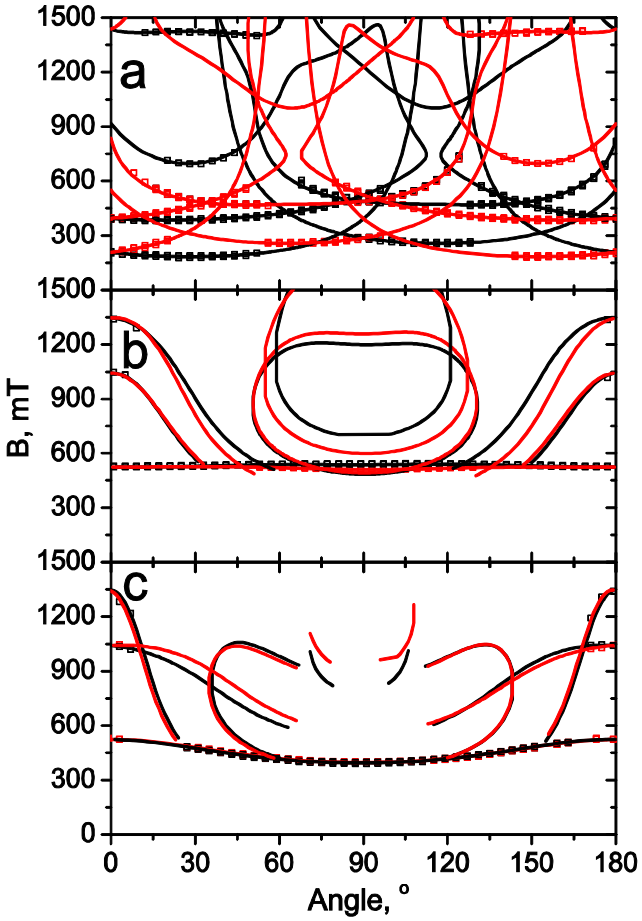

Figure 4: Angular dependence of the central EPR line positions (symbols) for the T1 centre in Q-band in three nearly perpendicular planes (a – bab, b – cbc and c – cac, $0°$ corresponding to b, c and c, respectively). Full lines represent simulations using the parameters in Table 2 and the two colours/symbols correspond to two symmetry related centres. Only transitions with probabilities larger than 10^{-4} of the most intense are shown.

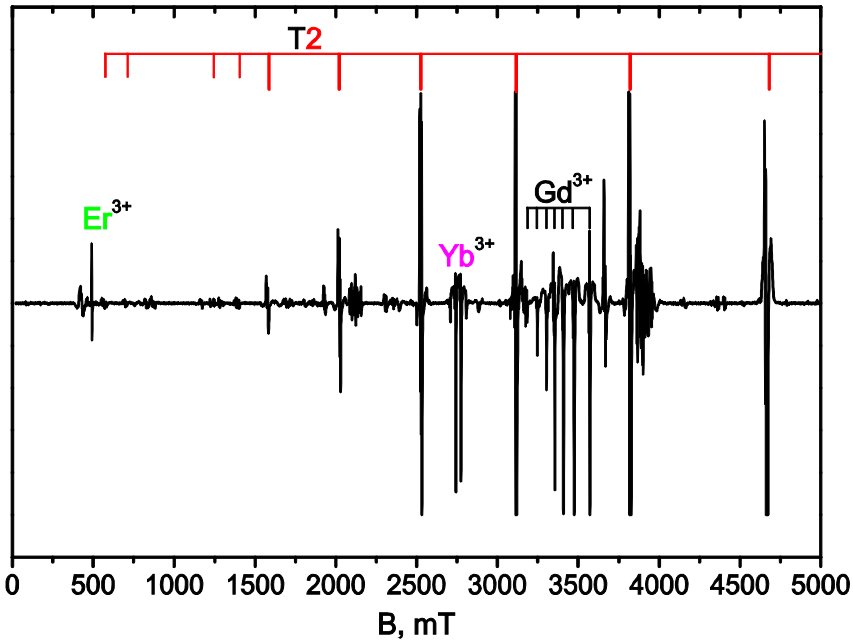

Figure 5: W-band EPR spectrum of K_2YF_5:Tb irradiated at T=77K and annealed to RT for several hours, recorded at T=10K and with the magnetic field along the *a*-axis. Signals of the Er^{3+}, Yb^{3+} and Gd^{3+} impurities and the radiation-induced T2 centre (bold tags for $\Delta M_S=1$ allowed and normal tags for forbidden transitions) are indicated in the spectrum. Unassigned transitions are most probably due to T3 and/or not completely annealed-out T1.

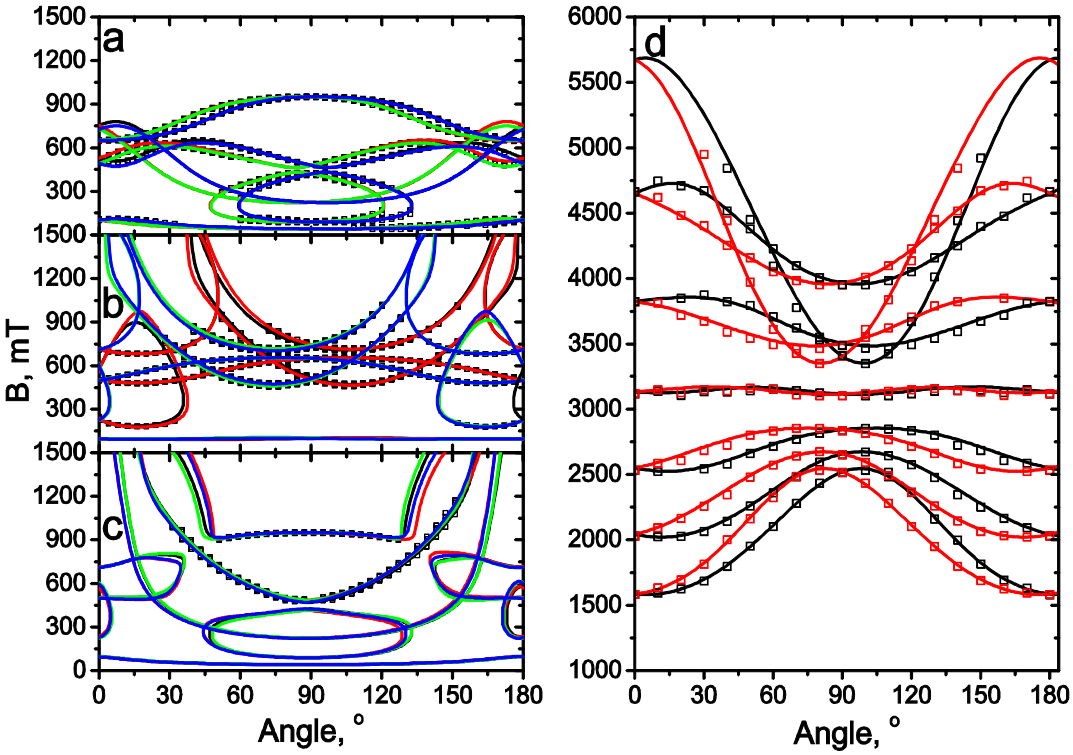

Figure 6: Angular dependence of EPR line positions (symbols) in three nearly perpendicular planes (a – *bab*, b – *cbc* and c – *cac*, with b, c and c at $0°$, respectively) at Q-band and one additional plane (d – *bab*, b at $0°$) at W-band for the T2 centre. Full lines represent simulations using the parameters in Table 2. Due to small mistiltings of the rotation planes all four symmetry related centres (different colours/symbols) can be observed in the Q-band angular dependences.